Simulating local mobility and mechanical properties of thermostable polyimides with different dianhydride fragments

Simulating local mobility and mechanical properties of thermostable polyimides with different dianhydride fragments

Victor M. Nazarychev,[1,*] Alexey Yu. Dobrovskiy,[2] Sergey V. Larin,[1] Alexey V. Lyulin,[3] Sergey V. Lyulin[1,2]

[1]Institute of Macromolecular Compounds, Russian Academy of Sciences, Bol'shoi pr. 31 (V.O.), St. Petersburg, 199004, Russia

[2]Faculty of Physics, St. Petersburg State University, Ul'yanovskaya str. 1, Petrodvorets, St. Petersburg, 198504, Russia

[3]Theory of Polymers and Soft Matter Group, Technische Universiteit Eindhoven, PO Box 513, 5600 MB Eindhoven, The Netherlands

Correspondence to: V. M. Nazarychev (E-mail: *nazarychev@imc.macro.ru*)

((Additional Supporting Information may be found in the online version of this article.))

ABSTRACT

The dynamic and mechanical properties of three thermoplastic polyimides, crystallizable polyimide BPDA-P3 and amorphous polyimides ODPA-P3 and aBPDA-P3, have been simulated using the atomistic molecular dynamics technique. The three simulated polyimides differ in the chemical structure of their corresponding dianhydride fragments. Analyzing the local orientational mobility of different phenyl rings, it has been established that the decrease of the glass-transition temperature (T_g) in the ordered set $T_g^{aBPDA-P3} > T_g^{BPDA-P3} > T_g^{ODPA-P3}$ is caused by the slowing down of the phtalimide rings relaxation in the corresponding dianhydride fragments. It has been observed that rather poor mechanic characteristics upon aBPDA-P3 stretching in the strain-hardening regime are also due to the low orientational mobility of the phtalimide rings. The correlation between the dynamic fragility and the polyimides strain-hardening moduli has been observed; the increase of the dynamic fragility leads to the increase of the strain-hardening modulus.

KEYWORDS: polyimides, local orientational mobility, glass transition temperature, fragility, strain-hardening modulus

INTRODUCTION

The nature of the transition from the liquid-like viscoelastic state to the solid-like glassy state in polymers melts remains a tremendous challenge in the condensed matter physics.[1,2] The characteristic feature of the glass transition is huge increase of the polymer-melt viscosity upon cooling down to the glass-transition temperature, T_g.[1,2] The value of T_g is governed by many different factors, as, for example, the polymer-specific chemical structure and the implemented cooling rates,[3] the polymer molecular weight,[4] the applied pressure,[5] etc. Both thermodynamic and kinetic approaches are used to describe the phenomenon.[1,2]

Thermodynamic theory of Adam and Gibbs[6] connects the glass transition with the abrupt change of the configurational entropy in the vicinity of T_g. Kinetic approaches which are mainly based on the general theory of mode coupling (the mode-coupling theory, MCT[7]), characterize the vitrification as a pure kinetic effect.[1,2]

Depending on the deviation of the temperature dependence for the viscosity $\eta(T)$,[8] or the structural relaxation time $\tau(T)$[9] from the Arrhenius behavior, all the materials belong to strong (small deviations observed above T_g) or fragile (large deviations) liquids.[9] Polymers are fragile, and show significant tremendous slowing down of structural relaxation. This slowing down of the segmental mobility upon approaching the T_g does not influence the chain conformations, they remain practically unchanged. The continuous nature of the glass transition can lead to the very strong correlation of the mechanical characteristics in the glassy state with those in the viscoelastic state. For example, Novikov and Sokolov[10] have shown that the correlation exists between the values of the Poisson ratio in the glassy state and the dynamic fragility m, which characterizes quantitatively the deviation of $\eta(T)$ and $\tau(T)$ from the Arrhenius law. For a very broad range of polymers the connection between the dynamic fragility and polymer mechanic characteristics has been investigated,[11] both above and below T_g. It was shown[11] that around T_g the different "glassy" polymer dynamic properties are correlated to their ability to create the additional free volume, that, in turn, depends on the fragile or strong nature of their corresponding liquids above T_g. Nevertheless, the question remains open how the polymer mechanics upon plastic deformation in the glassy state could be connected to the polymer relaxation processes taking place above T_g. To the best of our knowledge, such studies are absent at the moment.

The design of new thermoplastic heterocyclic polymers with improved mechanical properties is an important industrial challenge. Unfortunately, the question remains open on which changes in the polymer chemical structure lead to the improved thermal characteristics and, at the same time, do not decrease the mechanical performance in the glassy state. Among all the heterocyclic polymers, the thermoplastic polyimides (PI) are very suitable model objects for this type of research. Their repeated units contain conjugated aromatic rings which basically define their excellent thermal and good mechanical characteristics in the glassy state.[12-14] At the same time, the complicated PI chemical structure makes it very difficult to establish a direct correlation between the tiny chemical modifications with the corresponding changes of the thermal and mechanic polymer characteristics.

In particular, the very gentle change of the PI chemical structure can lead to the drastic change in its physical behavior. In our previous studies[15,16] the computer simulations have been carried out to investigate the thermal properties of several thermoplastic PI, both amorphous R-BAPS and R-BAPO, and semi-crystalline polyimide R-BAPB. These PIs differ in the chemical structure of the corresponding diamine fragments.[15,16] It was established that the different thermal properties of these PIs are caused by the differences in the backbone flexibility and by the different dipole-dipole interactions.

The thermal and mechanic properties have been simulated in [17] for PIs with different diamine fragments. The authors of [17] have shown that the decrease in the torsional mobility correlates rather strongly with the increase in the glass-transition temperature. At the same time, the PI mechanical properties in the glassy state remain basically unaffected. The connection between the orientational mobility of different repeated PI fragments at T_g, and the PI mechanical behavior, remains unclear.

In the present study the local orientational mobility has been simulated in the polyimides aBPDA-P3, BPDA-P3 and ODPA-P3. These PIs are based on three dianhydrides, 3,3',4,4'-oxidiphthalic dianhydride (ODPA), 2,3',3,4'-biphenyltetracarboxylic dianhydride (aBPDA) and 3,3',4,4'-biphenyltetracarboxylic dianhydride (BPDA), and diamine 1,4-bis[4-(4-aminophenoxy)phenoxy]benzene (P3). The possible correlation has been studied between the orientational relaxation above T_g and the PI mechanical characteristics. The main attention has been paid to the properties of the semicrystalline thermoplastic PI BPDA-P3.[18] The chemical structure of its dianhydride fragment in this polymer includes a rigid spacer between two phtalimide rings, similar to the structure of the diamine fragment of R-BAPB.[19] In this paper we simulated the differences in the orientational relaxation of vectors normal to the phenylene (PH_1-PH_5) and phtalimide (PH_6 and PH_7) rings in BPDA-P3 and ODPA-P3, for the later the dianhydride fragment contains flexible oxygen junction. The comparison has also been made with the orientational segmental relaxation in aBPDA-P3. For this PI phtalymide rings in the corresponding dianhydride fragments are connected asymmetrically,[18,20] Figure 1.

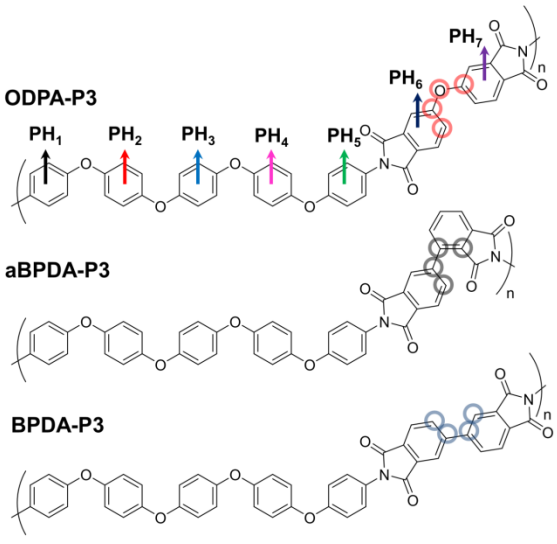

FIGURE 1. The chemical structure of the simulated thermoplastic PI repeated units ODPA-P3, aBPDA-P3 and BPDA-P3. The arrows indicate the normal vectors to the planes of the phenyl and phtalimide PH_1-PH_7 rings, their orientational mobility has been studied in this paper. For clarity these vectors are not shown for aBPDA-P3 and BPDA-P3. The circles define the dihedral angles studied in the paper.

We believe that the simulations of the local orientational mobility can shed light onto the influence of the dianhydride fragments chemical structure on PI dynamic properties above T_g, as well as on their mechanical characteristics in the irreversible plastic deformation region. The comparison of the thermomechanics of BPDA-P3 with that of ODPA-P3 и aBPDA-P3 is carried out for the samples with and without partial charges. This will allow us to establish the influence of the dipole-dipole interactions on the properties of the simulated polyimides. We hope that the results and the main conclusions of this study can provide useful insights for the future design of new thermoplastic heterocyclic polymers with improved both thermal and mechanical characteristics.

MODELS UNDER STUDY AND DETAILS OF THE COMPUTER SIMULATIONS

The initialization and building of the ODPA-P3, aBPDA-P3, and BPDA-P3 simulation boxes have been carried out during the microsecond-long run using the earlier developed approach.[15,16,21-27] At the very beginning, 27 partially-coiled PI chains with the polymerization degree N_p=8 have been placed randomly (avoiding overlaps and entanglements) into the cubic box. Each polymer chain of aBDPA, BPDA-P3 and ODPA-P3 has 17766, 17766 and 17982 atoms correspondingly. The length of periodic box side for each of thermostable polyimides at T=600 K was in the range from 6.0-6.1 nm. In our previous study[24,34], we showed, that polymerization degree N_p=8 is suitable to predict correctly thermal (glass-transition temperature) and mechanical properties

(Young's modulus) of thermoplastic polyimides R-BAPS and R-BAPO, which corresponds approximately 15 Kuhn segments. Therefore in this work we chose the same polymerization degree. Periodic boundary conditions have been used in all three directions. The modelling have been performed with and without Coulombic interactions (in the latter case the partial charges were all set to zero) in order to study the influence of the dipole-dipole interactions on the thermal and mechanical properties of the simulated PIs. The values of the partial charges have been calculated using the Hartree-Fock method with 6-31G* basis.[15] Calculated values of partial charges for BPDA-P3, ODPA-P3, and aBPDA-P3 could be found in the Supporting Information, See Figure S1 and Table S1-S3. The electrostatic interactions have been taken into account with the help of the Particle Mesh Ewald (PME) algorithm.[28] Temperature and internal pressure are both kept constant using Berendsen thermostat and barostat[29] with parameters τ_t=0.1 ps and τ_p=0.5 ps for thermostat and barostat relaxation times, correspondingly. The computer simulations have been performed using Gromacs molecular-dynamics software[30,31] and Gromos53a5 force field.[32] This force field has been successfully implemented by the authors in their previous simulations of both structure and the thermal properties of different thermoplastic polyimides.[15,16,21-27]

The short simulation run of about 26 ns was used to compress the initially created boxes. To remove the residual stresses, the box annealing procedure has been performed. Namely, three repeated cycles of consequent cooling down and heating up between 800 K and 300 K have been carried out. After this annealing the instant quenching from 800 K to 600 K has been realized. The equilibration runs have been continued at this temperature, T=600 K, for another 1.5 μs. During this time the average chain dimensions reach their equilibrium time-independent values which were in a very good agreement with the theoretical estimations (see Figure S2 in the Supporting Information). The production runs follow the equilibration for another 1.5 μs. The last 1 μs of the production run has been used to save 11 consequent instant system configurations every 100 ns of the simulated trajectory for further analysis.

To study the thermal characteristics, both samples with and without partial charges have been heated up to 800 K and have been simulated for 100 ns. After that the step-wise cooling have been carried out from 800 K to 290 K with the cooling velocity γ_c=1.5×10^{11} K/min. The melt density has been monitored during this cooling; the temperature dependence of the simulated density was used to measure the T_g values together with the coefficient of thermal expansion (CTE).

T_g values have been produced using the linear approximations of the temperature-density plots in both high- and low-temperatures regions. CTE coefficients β have been calculated using

$$\beta = \frac{1}{\rho_1}\frac{(\rho_2 - \rho_1)}{(T_2 - T_1)}, \qquad (1)$$

Where ρ_1 and ρ_2 are the PI density at temperatures T_1 and T_2 separated by 10 K.

During the cooling step the local orientational mobility of the phenyl rings normal vectors have been simulated, both for the diamine (PH_1-PH_5) and for the dianhydride (PH_6 and PH_7) fragments of the repeated unit, Figure 1. The first-order Legendre polynomials $P_1(t)$ have been calculated for these vectors,[33]

$$P_1(t) = \langle \mathbf{b}(0)\mathbf{b}(t) \rangle, \qquad (2)$$

Where $\mathbf{b}(0)$ and $\mathbf{b}(t)$ are the corresponding normal vectors at the beginning (t=0) and at the current moment of time t. The angular brackets $\langle ... \rangle$ denote the averaging over all 216 rings of 11 independent samples.

The obtained $P_1(t)$ dependences for aBPDA-P3, ODPA-P3, and BPDA-P3 PIs have been approximated by the Kohlraush-Williams-Watts (KWW) stretched exponentials,[33]

$$P_1(t) = A\exp\left(-(t/\tau)^{\beta}\right), \quad (3)$$

where A ≤ 1, τ is the characteristic relaxation time and β is the stretching parameter taking into account the nonexponentiality of the relaxational process. The KWW relaxation times τ were used to calculate the averaged times τ_{rot} of the rotational relaxation as

$$\tau_{rot} = \frac{\tau_{KWW}}{\beta}\Gamma\left(1/\beta\right), \quad (4)$$

where $\Gamma(\ )$ is gamma function.

200-ns trajectories at T=600 K have been used to calculate the autocorrelation functions $C_{\chi}(t)$ for the dihedral angles relaxation as[17]

$$C_{\chi}(t) = \left\langle \cos\left[\chi(\tau) - \chi(\tau + t)\right]\right\rangle_{\tau}. \quad (5)$$

Where χ is the dihedral angle. To study the possible correlation between the high-T local segmental mobility and the low-T mechanical properties, the simulated PI samples have been deformed uniaxially at the room temperature T=290 K using the approach suggested by us earlier.[34] Before the simulations of the uniaxial stretching the LINCS algorithm[35] fixing the chemical bonds has been switched off. Instead, the harmonic potential of the Gromos53a5 force field has been implemented. After this modification the additional equilibration for another 400 ps has been done. The LINCS algorithm did not taking into the account due to the observed instability of simulations on a multiprocessor system upon high-speed deformation. The difference between calculated mechanical properties for samples with and without LINCS is not more the 5 %, see Figure S3 in Supporting Information.

The uniaxial deformation consists of the affine deformation of the simulated box along the positive direction of one of the axes (X, Y or Z) with some constant velocity.[36] Anisotropic Berendsen barostat with the relaxation time τ_p=1 ps was used at this stage.[29] The condition of uncompressibility was used in the direction of the deformation, the compressibility in the perpendicular direction was fixed at 4.5×10^{-10} Pa^{-1} which is the default compressibility value in the Gromacs package. The transversal cell dimensions were not fixed and were allowed to change in response to the external pressure. All the deformation experiments have been carried out with fixed deformation rate of γ_d = 1.8×10^{8} s^{-1}.[34,37,38]

The diagonal components of the stress tensor P_i, *i={x, y, z}*, have been saved every 1 ps. The values of P_i and the periodic cells dimensions were calculated using the gmx energy routine of the Gromacs package. The calculated values were used to produce the stress-strain dependence as:[39]

$$\sigma = -P_i, \qquad \varepsilon = \frac{L_i - L_{0i}}{L_{0i}}, \quad (6)$$

where L_{0i} is the cell dimensions at the start of the deformation, (t=0).

Initially, the dependence *σ(ε)* is very close to linear; this linear viscoelastic regime is clearly observed up to ~2% of the deformation *ε*,[39] and was used to extract the Young modulus *E* as

$$\sigma = E\varepsilon, \quad (7)$$

In order to calculate the yield stress σ_y and the strain hardening modulus G_h the dependence *σ(ε)* was converted from the engineering stress-strain dependence (*ε=λ-1*) to Gaussian-based stress-strain dependence ($\varepsilon_t=\lambda^2-\lambda^{-1}$), where $\lambda=L_i/L_{0i}$. The simulated the yield stress and the strain-hardening modulus were calculated from

$$\sigma(\varepsilon_t) = \sigma_Y + G_h(\varepsilon_t) \quad (8).$$

RESULTS AND DISCUSSION

After the 3 μs equilibration at high temperature, T=800K, the PI samples have been cooled down to the room temperature, T=290K. The simulated glass-transition temperatures for the samples with and without partial charges correlate very well with the experimentally observed ordered set for the considered PIs, $T_g^{aBPDA-P3} > T_g^{BPDA-P3} > T_g^{ODPA-P3}$, see the Supporting Information Figure S4a and Table S4. The CTE values for the PI samples with and without partial charges are very close to each other, see the Supporting Information Fig. S4b and Table S4.

The preliminary cooled (cooling velocity is γ_c = 1.5×10^{11} K/min) PI samples, both with and without partial charges, have been uniaxially deformed with the deformation rate of γ_d~1.8×10^8 s^{-1} at T=290 K. The simulated stress-strain curves are shown in Figure 2.

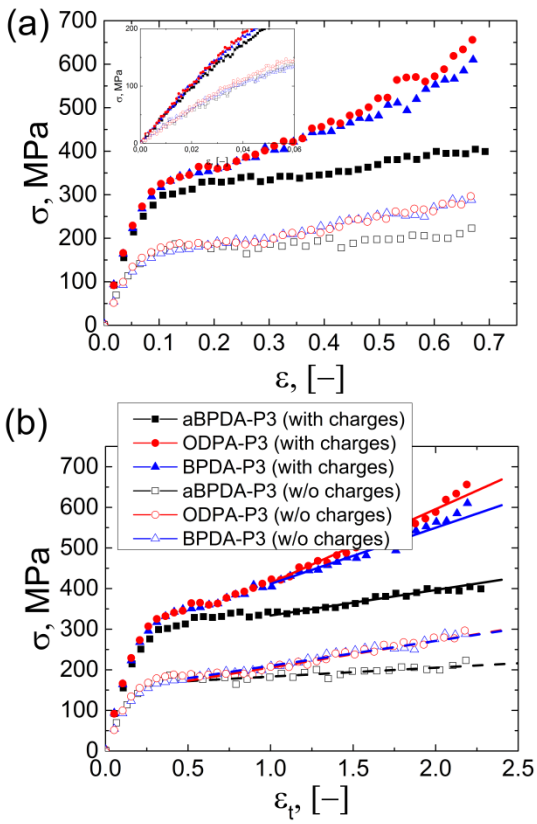

FIGURE 2. (a) The stress-strain dependence for the simulated PIs (ODPA-P3, aBPDA-P3 and BPDA-P3) with and without partial charges. The insert shows the region of the linear response. (b) The same, but in terms of the Gaussian-based stress-strain dependence, $\varepsilon_t=\lambda^2-\lambda^{-1}$. Continuous and dashed lines are fits with Eq. (8) for the samples with and without partial charges, correspondingly.

The analysis of the stress-strain dependences of the simulated PIs shows that for the samples with partial charges and with proper accounting of the Coulombic interactions the values of the Young modulus and the yield stress are almost twice larger as compared to those without partial charges, Figure 2a. Small deformations below 10% produce almost identical stress-strain characteristics for all the simulated samples. The further stretching, at ε > 0.15, shows much lower stress for aBPDA-P3 as compared to the corresponding values for ODPA-P3 and BPDA-P3. We can speculate here that this lower stress response can be connected to the slowing down of the segmental relaxation of dianhydride fragments for this PI as compared to the mobility of the phtalimide fragments in ODPA-P3 and BPDA-P3 (see discussion later). The lower segmental relaxation of dianhydride fragments for aBPDA-P3 might be due to decreasing of its average radius of gyration and the end-to-end distance in comparison to sizes for ODPA-P3 and BPDA-P3, see Figure S2 in Supporting Information.

The decrease of polymer chain size of aBPDA-P3 could be related to bend of aBPDA-P3 polymer chains, see Figure S2, which might to lead to decrease of number of entanglements between the chains. We used QSPR analysis with help of Materials Studio to estimate the number of entanglements per chain for three considered PIs. The results have shown that aBPDA-P3 has ~1.3 entanglements per chain and BPDA-P3 and ODPA-P3 have ~1.5 entanglements per chain. Thus, the PI aBPDA-P3 has a few less entanglements per one polymer chain in comparison to ODPA-P3 and BPDA-P3. This may lead to decrease aBPDA-P3 strain-hardening

modulus in comparison to values of strain-hardening modulus of two others PIs.Note that the simulated mechanical characteristics, Table 1, are in a good agreement with the experimental data. Hegde et al.[18,20] showed that bulk aBPDA-P3, ODPA-P3 and BPDA-P3 samples have very similar Young moduli, E ~2.6-2.8 GPa.

TABLE 1. The Young moduli values for the simulated thermoplastic PIs aBPDA-P3, BPDA-P3 and ODPA-P3 with and without partial charges calculated from the stress-strain dependences in Figure 2.

PIs	Elastic modulus, E, GPa with partial charges	without partial charges
aBPDA-P3	5.0 ± 0.2	3.0 ± 0.2
ODPA-P3	5.2 ± 0.2	3.1 ± 0.2
BPDA-P3	5.3 ± 0.2	3.1 ± 0.2

The very similar (for all three PIs) simulated results, Table 1, are in a qualitative agreement with experiment.[18,20] The larger - compared to the experimental data - absolute simulated values are connected to the logarithmic dependence[37] of the Young modulus on the cooling and deformation velocities; the simulated rates are inevitably much higher.

In current study using logarithmic dependence, we extrapolated Young's modulus value to experimental deformation rate, Figure S5a,b in Supporting Information. Due to the high difference (close to 10-14 orders) between the deformation rates in computer simulation (γ_d^{sim}=1.8×(10^6-10^{10}) s^{-1}) and experiment (γ_d^{exp}=5.5×10^{-5} s^{-1}) we predict by extrapolation the experimental Young's modulus value that much lower (0.15 GPa) than experimental one (E=2.8 GPa). The difference between the experimental and simulation values of Young's modulus is could be related to influence of cooling rate on value of Young's modulus. As was shown in our previous paper[34] Young's modulus also depends logarithmically on the cooling rate (the lower is cooling rate, the higher is Young's modulus). And if we also make extrapolation to experimental cooling rate (γ_c ~ 5 K/min) we might obtain the value of Young's modulus close to experiment one. However, the error in calculation of Young's modulus might be rather height. The model with partial charges, that gave higher Young's modulus (E=0.15 GPa) in comparison to model without partial charges (E=-1.2 GPa), might be more realistic to reproduce experimental value of Young's modulus, Figure S5c in Supporting Information. Note, nevertheless, that such conclusion should be taken with some caution, as it has only some qualitative character. To do quantitative compare computer simulation results and experimental data one should use simulations with much slower cooling rates γ_c.

The fitting of the $\sigma\left(\lambda^2-\lambda^{-1}\right)$ dependences using Eq. (8), Figure 2c, the yield peak values σ_y and the strain hardening moduli of the simulated polymers can be calculated, Table 2.

TABLE 2. The yield peak and the strain hardening moduli for aBPDA-P3, ODPA-P3 and BPDA-P3 with and without partial charges.

PIs	σ_y, MPa with partial charges	without partial charges	G_h, MPa with partial charges	without partial charges
aBPDA-P3	271 ± 3	161 ± 2	63 ± 2	22 ± 1
ODPA-P3	232 ± 2	140 ± 2	182 ± 1	66 ± 1
BPDA-P3	273 ± 2	149 ± 2	139 ± 3	61 ± 1

Comparing the stress-strain curves in Figure 2c and the values of the strain-hardedning moduli in Table 1 we can conclude that the presence of the asymmetric dianhydride fragment in the repeated unit of aBPDA-P3 results in the smaller strain-hardening modulus, the corresponding moduli for BPDA-P3 и ODPA-P3 are larger. We can speculate that this difference in both thermal and mechanical properties of the simulated polyimides is mainly due to the difference in the mobility of phtalimide rings, and the differences in the characteristic polymer dimensions, as explained earlier.

The local orientational mobility of different phenyl rings has been directly simulated. The typical dependences $P_1(t)$ for the PI samples with and without partial charges are shown in

Figure S6 in the Supporting Information. Similar to the previous results published for R-BAPS,[37] the explicit partial charges lead to the significant (by app. two orders of magnitude) slowing down of the local orientational mobility. It has been established that the symmetric phenyl rings PH_2, PH_3 and PH_4 have very similar relaxational characteristics, the corresponding $P_1(t)$ are almost identical. To have better statistics, the simulated relaxation times for the normal vectors have been averaged over all the rings in the samples of each PI, in the centers of the diamine fragments, PH_2, PH_3, PH_4, and at the edges, PH_1 and PH_5. The relaxation times for the phtalimide rings PH_6 и PH_7 in the dianhydride fragments have been averaged as well. In what follows we will use the notation (for example) $PH_{2,3,4}$ to show that the averaging was carried out for the normal vectors to the planes of the rings PH_2, PH_3, PH_4.

Note here that the temperature dependences of the relaxation times calculated for PI models with and without (Figure 3) partial charges by their tendency are similar to each other. Using the stretched exponentials fitting (eq. 3) for the averaged autocorrelation functions $P_1(t)$ the temperature dependence of the averaged relaxation times $\tau_{rot}(T)$ have been defined,[37] Figure 3.

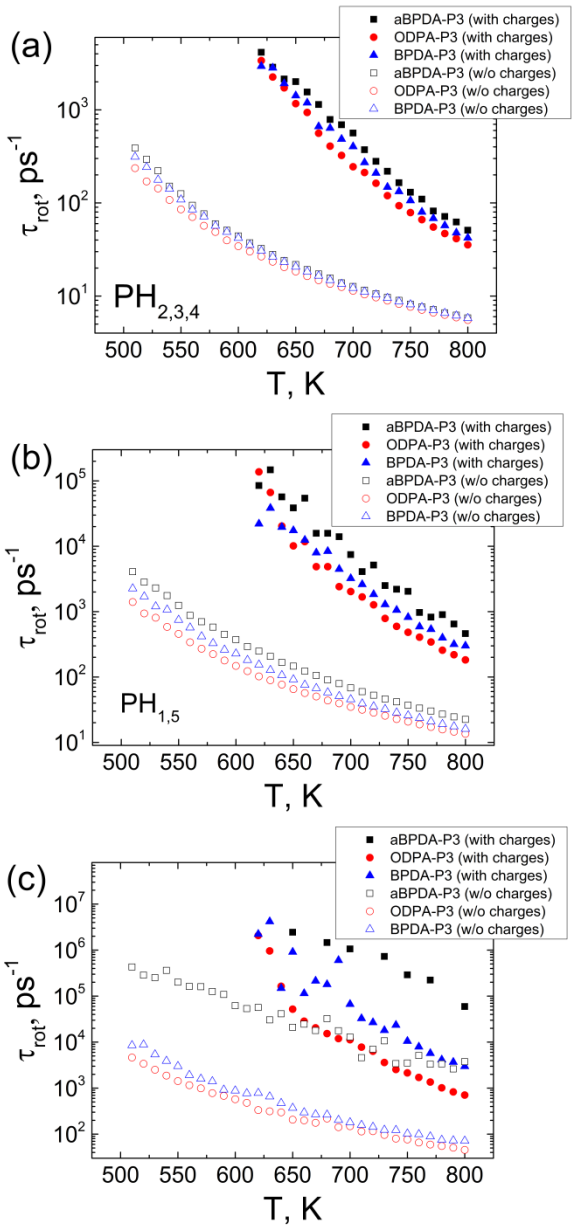

FIGURE 3. The temperature dependence of the averaged relaxation times for the orientational mobility of the normal vectors for the PI samples with and without partial charges; (a) for the phenyl rings $PH_{1,5}$; (b) for the phenyl rings $PH_{2,3,4}$; (c) for the phtalimide rings $PH_{6,7}$.

The analysis of the results in Figure 3 shows that the temperature dependences of the averaged relaxation times $\tau_{rot}(T)$ for the phenyl rings $PH_{2,3,4}$ are very similar to each other. The relaxation of the phenyl rings $PH_{1,5}$

attached to the dianhydride fragment are only slightly different, Figure 3a; this reflects the direct influence of the dinnhydride fragments on the phenyl rings relaxation. The relaxation of the phtalimide rings $PH_{6,7}$ is the most different among the simulated polymers. The averaged relaxation times for $PH_{6,7}$ rings in the aBPDA dianhydride fragment are about two orders of magnitude larger as compared to the relaxation times of the rings in the corresponding fragments of BPDA-P3 и ODPA-P3 polyimides, Figure 3c. The presence of the flexible oxygen junction in the ODPA-P3 dianhydride fragment facilitates the enhanced mobility. The mobility of the phtalimide rings in BPDA-P3 is slightly larger as compared to that in aBPDA-P3 polymer. The ordering of the orientational relaxation times, $\tau_{rot}^{aBPDA-P3}(T) > \tau_{rot}^{BPDA-P3}(T) > \tau_{rot}^{ODPA-P3}(T)$, correlates with the ordering of the corresponding glass-transition temperatures, T_g: $T_g^{aBPDA-P3} > T_g^{BPDA-P3} > T_g^{ODPA-P3}$; the most decelerated mobility is observed in PIs with the largest T_g.

This difference in the segmental relaxation of dianhydride fragments can be connected with some structural difference in the corresponding dihedral angles, Figure 1. In Figure 4 the distribution functions of the dihedral angles in the dianhydride fragments are presented, as well as the corresponding autocorrelation functions. $C_\chi(t)$ at T=600 K.

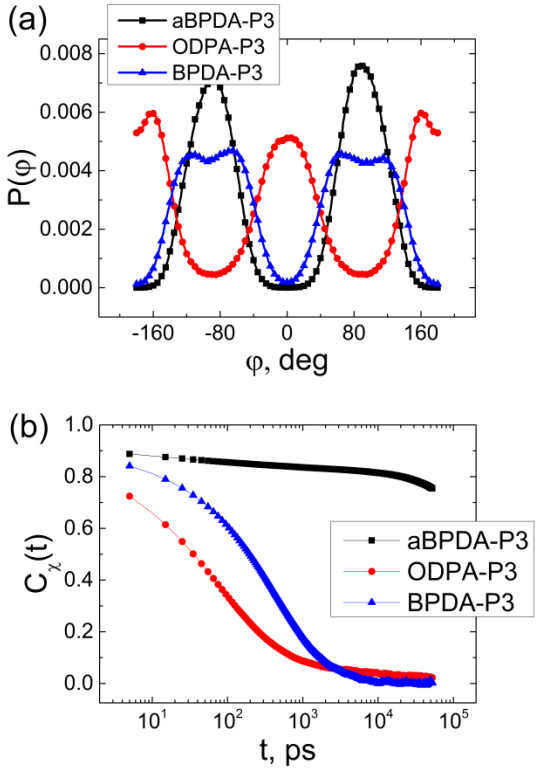

FIGURE 4. (a) Distribution functions for the dihedral angles in the dianhydride fragments (see Figure 1) of aBPDA-P3, ODPA-P3, and BPDA-P3. (b) Time dependence of the corresponding autocorrelation functions $C_\chi(t)$ for the three PIs. T=600 K.

It is seen that the phtalimide cycles in aBPDA-P3 are perpendicular to each other, Figure 4. The distribution function for the dianhydride in BPDA-P3 shows two maxima, at χ ~ 60° and 120°. Finally, the same distribution function for ODPA-P3 also has two maxima, but at χ ~160° and ~ 0°, which reflects the almost planar structure of the ODPA-P3 dianhydride fragments, Figure 4a. The perpendicular orientation of the phtalimide rings in aBPDA-P3 hinder the orientational relaxation significantly, planar structure of the corresponding fragments in ODPA-P3 significantly enhances the orientational mobility, Figure 4b. As seen from the data in Figure 3 and Figure 4 the difference in the orientational mobility exists only for the phtalimide rings, this, from our point of view, could lead to the significant

difference in the glass transition temperatures of these polymers.

The temperature dependences of the phtalimide rings PH_6 and PH_7 orientational relaxation times $\tau_{rot}(T)$ was used to estimate the dynamic fragility of the simulated polymers. The high-temperature (from 650 K to 800 K for samples without partial charges and for 730 K to 800 K for samples without partial charges) parts of the $\tau_{rot}(T)$ dependences were approximated by the Arrhenius law, $\tau = \tau_0 \exp(E/T)$, where τ_0 is some time characterizing fast relaxation close to the local potential minima, and E is an activation energy. The dynamic fragility m[10] was calculated using the simulated T_g data from the Table S3 in the Supporting Information,

$$m = \frac{(19.2)^2 \ln 10}{E} T_g \qquad (9)$$

The simulated activation energies and the dynamic fragilities are summarized in Table 3.

TABLE 3. The activation energy for the orientational relaxation of $PH_{6,7}$ phenylene ring and the corresponding dynamic fragility of aBPDA-P3, ODPA-P3 and BPDA-P3 with and without partial charges.

PIs	E, J·K/mol		m	
	with partial charges	without partial charges	with partial charges	without partial charges
aBPDA-P3	$2.0 \cdot 10^4$	$0.7 \cdot 10^4$	26	63
BPDA-P3	$1.6 \cdot 10^4$	$0.6 \cdot 10^4$	33	70
ODPA-P3	$1.3 \cdot 10^4$	$0.5 \cdot 10^4$	40	82

The largest fragility is observed for ODPA-P3. The increase of T_g at the same time leads to the decrease in fragility, aBPDA-P3 is stronger liquid, and ODPA-P3 и BPDA-P3 are more fragile.

The analysis of the results in Tables 1 and 3 clearly shows the correlations between the dynamic fragility and the strain hardening moduli. The ordering of the strain-hardening moduli, $G_h^{aBPDA-P3} < G_h^{BPDA-P3} < G_h^{ODPA-P3}$, is the same as the ordering of the corresponding dynamic fragilities, $m^{aBPDA-P3} < m^{BPDA-P3} < m^{ODPA-P3}$. The observed slowing down of the dianhydride fragments relaxation leads to the increase of the glass transition temperature and to the decrease of the dynamic fragility and to the decrease of the strain-hardening moduli of the simulated polyimides. The simulations show that BPDA-P3 has the best thermal and mechanical characteristics, with high enough the glass-transition temperature and large strain-hardening modulus. The values of Young modulus for all three polymers are comparable. However, qualitatively the direction of changes of thermal and mechanical characteristics for three PIs is rather similar for both models. Namely, the ratio between temperature dependences of relaxation times τ(T) for three considered PIs, thermal (glass transition temperature, T_g,) and mechanical (strain-hardening modulus, G_h) characteristics are almost the same for models with and without partial charges. This conclusion may be related with the absence of strong polar groups in the chemical structure of the PIs. This may be due to the fact, that three considered PIs in their chemical structure do not have polar groups. Therefore, to investigate qualitatively difference between properties PIs, that chemical structure does not consist polar groups one could perform less resource-intensive computer simulation without partial charges. However, as have been shown early in our previous study[37] the systems with partial charges much better reproduce experimental value of mechanical characteristics if we do extrapolation both for cooling and deformations rates to experimental deformation rates. And if we do extrapolation to experimental deformation and cooling rates, the model with partial charges qualitatively predicts close Young's modulus values in computer simulation to experimental results in comparison to results for model without partial charges.

CONCLUSIONS

In this manuscript the μs-long atomistic molecular-dynamic simulations have been carried out to study the dynamic and mechanical properties of three important thermoplastic polyimides: aBPDA-P3, ODPA-P3, and BPDA-P3. We have shown that the local orientational mobility in the dianhydride fragments of the simulated aBPDA-P3 samples is about two orders of magnitude slower as compared to the mobility of the phtalimide fragments in ODPA-P3 and BPDA-P3. We have established the correlation between the slowing down of the local orientational mobility of the phtalimide rings of the dianhydride fragments of the PI repeated units and PI mechanical properties. The low orientational mobility of the dianhydride fragments in aBPDA-P3 is caused by the asymmetric configurations of its phtalimide rings and leads to the lowest (among the simulated PIs) values of dynamic fragility and the strain-hardening modulus.

The 90° orientation of the phtalimide rings in the asymmetric dianhydride of aBPDA-P3 leads to the significant slowing down of their relaxation as compared to the relaxation of the phtalimide rings in the BPDA-P3 dianhydride, and in ODPA-P3 where the additional oxygen atom of dianhydride accelerates the orientational relaxation. The presence of the asymmetric dianhydride aBPDA leads to the significant decrease of the strain-hardening modulus for aBPDA-P3. The presence of the flexible oxygen junction in the dianhydride ODPA increases the orientational relaxation in ODPA-P3 polyimide which, in turns, decreases the glass-transition temperature. The symmetric dianhydride BPDA keeps the BPDA-P3 mechanical properties comparable to those of ODPA-P3, at the same time leads to the increase in the glass-transition temperature.

The conclusions of the present study can be used to provide some insights and directions for the design of novel thermostable heterocyclic polymers with increased toughness and improved mechanical characteristics in the regime of plastic deformations.

ACKNOWLEDGEMENTS

V.M. Nazarychev and A.Yu. Dobrovskyi acknowledge the financial support from the President of Russian Federation Grant (agreement No. 14.W01.17.2140-MK). All the simulations have been performed using the computational resources of the Institute of Macromolecular Compounds, Russian Academy of Sciences, the equipment of the shared research facilities of HPC computing resources at Lomonosov Moscow State University, and resources of the federal collective usage center Complex for Simulation and Data Processing for Mega-science Facilities at NRC "Kurchatov Institute" (http://ckp.nrcki.ru/).

REFERENCES AND NOTES

1. Binder, K., Kob, W. Glassy Materials and Disordered Solids: An Introduction to Their Statistical Mechanics, World Scientific, Singapore, 2011.
2. Debenedetti, P. G. Metastable Liquids: Concepts and Principles, Princeton University Press, Princeton, 1996.
3. Moynihan, C. T., Easteal, A. J., Wilder, J., Tucker, J. *J. Phys. Chem.*, 1974, **78**, 2673–2677.
4. Fox, T. G., Flory, P. J. *J. Polym. Sci.*, 1954, **14**, 315–319.
5. Harmandaris, V. A., Floudas, G., Kremer, K. *Macromolecules*, 2011, **44**, 393–402.
6. Adam, G., Gibbs, J. H. *J. Chem. Phys.*, 1965, **43**, 139-146.
7. Cummins, H. Z. *J. Phys. Condens. Matter*, 1999, **11**, A95–A117.
8. Angell, C. A. *J. Phys. Chem. Solids*, 1988, **49**, 863–871.
9. Huang, D., McKenna, G. B. *J. Chem. Phys.*, 2001, **114**, 5621–5630.
10. Novikov, V. N., Sokolov, A. P. *Nature*, 2004, **431**, 961–963.
11. Wu, J., Huang, G., Qu, L., Zheng, J. *J. Non. Cryst. Solids*, 2009, **355**, 1755–1759.

12. Bessonov, M. I., Koton, M. M., Kudryavtsev, V. V., Laius, L. A. Polyimides: Thermally Stable Polymers, Plenum, New York, NY, 1987.
13. Ghosh, M. Polyimides: Fundamentals and Applications, CRC Press, 1996.
14. Rusanov, A. L. Practical Guide to Polyimides, iSmithers Rapra Publishing, Shawbury, 2007.
15. Nazarychev, V. M., Larin, S. V., Yakimansky, A. V., Lukasheva, N. V., Gurtovenko, A. A., Gofman, I. V., Yudin, V. E., Svetlichnyi, V. M., Kenny, J. M., Lyulin, S. V. *J. Polym. Sci. Part B: Polym. Phys.*, 2015, **53**, 912–923.
16. Falkovich, S. G., Lyulin, S. V., Nazarychev, V. M., Larin, S. V., Gurtovenko, A. A., Lukasheva, N. V., Lyulin, A. V. *J. Polym. Sci. Part B: Polym. Phys.*, 2014, **52**, 640–646.
17. Pandiyan, S., Parandekar, P. V., Prakash, O., Tsotsis, T. K., Nair, N. N., Basu, S. *Chem. Phys. Lett.*, 2014, **593**, 24–27.
18. Hegde, M., Lafont, U., Norder, B., Samulski, E. T., Rubinstein, M., Dingemans, T. J. *Polymer*, 2014, **55**, 3746–3757.
19. Yudin, V. E., Feldman, A. Y., Svetlichnyi, V. M., Shumakov, A. N., Marom, G. *Compos. Sci. Technol.*, 2007, **67**, 789–794.
20. Hegde, M., Lafont, U., Norder, B., Picken, S. J., Samulski, E. T., Rubinstein, M., Dingemans, T. *Macromolecules*, 2013, **46**, 1492–1503.
21. Lyulin, S. V., Larin, S. V., Gurtovenko, A. A., Lukasheva, N. V., Yudin, V. E., Svetlichnyi, V. M., Lyulin, A. V. *Polym. Sci. Ser. A*, 2012, **54**, 631–643.
22. Nazarychev, V. M., Larin, S. V., Lukasheva, N. V., Glova, A. D., Lyulin, S. V. *Polym. Sci. Ser. A*, 2013, **55**, 570–576.
23. Lyulin, S. V., Gurtovenko, A. A., Larin, S. V., Nazarychev, V. M., Lyulin, A. V. *Macromolecules*, 2013, **46**, 6357–6363.
24. Lyulin, S. V., Larin, S. V., Gurtovenko, A. A., Nazarychev, V. M., Falkovich, S. G., Yudin, V. E., Svetlichnyi, V. M., Gofman, I. V., Lyulin, A. V. *Soft Matter*, 2014, **10**, 1224–1232.
25. Larin, S. V., Falkovich, S. G., Nazarychev, V. M., Gurtovenko, A. A., Lyulin, A. V., Lyulin, S. V. *RSC Adv.*, 2014, **4**, 830–844.
26. Larin, S. V., Glova, A. D., Serebryakov, E. B., Nazarychev, V. M., Kenny, J. M., Lyulin, S. V. *RSC Adv.*, 2015, **5**, 51621–51630.
27. Falkovich, S. G., Larin, S. V., Lyulin, A. V., Yudin, V. E., Kenny, J. M., Lyulin, S. V. *RSC Adv.*, 2014, **4**, 48606–48612.
28. Darden, T., York, D., Pedersen, L. *J. Chem. Phys.*, 1993, **98**, 10089–10092.
29. Berendsen, H. J. C., Postma, J. P. M., van Gunsteren, W. F., DiNola, A., Haak, J. R. *J. Chem. Phys.*, 1984, **81**, 3684–3690.
30. Van Der Spoel, D., Lindahl, E., Hess, B., Groenhof, G., Mark, A. E., Berendsen, H. J. C. *J. Comput. Chem.*, 2005, **26**, 1701–1718.
31. Hess, B., Kutzner, C., van der Spoel, D., Lindahl, E. *J. Chem. Theory Comput.*, 2008, **4**, 435–447.
32. Oostenbrink, C., Villa, A., Mark, A. E., Van Gunsteren, W. F. *J. Comput. Chem.*, 2004, **25**, 1656–1676.
33. Lyulin, A. V, Balabaev, N. K., Michels, M. A. J. *Macromolecules*, 2002, **35**, 9595–9604.
34. Nazarychev, V. M., Lyulin, A. V., Larin, S. V., Gurtovenko, A. A., Kenny, J. M., Lyulin, S. V. *Soft Matter*, 2016, **12**, 3972–3981.
35. Hess, B., Bekker, H., Berendsen, H. J. C., Fraaije, J. G. E. M. *J. Comput. Chem.*, 1997, **18**, 1463–1472.
36. Lyulin, A. V., Balabaev, N. K., Mazo, M. A., Michels, M. A. J. *Macromolecules*, 2004, **37**, 8785–8793.
37. Nazarychev, V. M., Lyulin, A. V., Larin, S. V., Gofman, I. V., Kenny, J. M., Lyulin, S. V. *Macromolecules*, 2016, **49**, 6700–6710.
38. Falkovich, S. G., Nazarychev, V. M., Larin, S. V., Kenny, J. M., Lyulin, S. V. *J. Phys. Chem. C*, 2016, **120**, 6771–6777.
39. Ward, I. M., Sweeney, J. Mechanical

Properties of Solid Polymers, John Wiley & Sons, Ltd, Chichester, UK, 2012.

GRAPHICAL ABSTRACT

Victor M. Nazarychev, Alexey Yu. Dobrovskiy, Sergey V. Larin, Alexey V. Lyulin, Sergey V. Lyulin

Simulating local mobility and mechanical properties of thermostable polyimides with different dianhydride fragments

The dynamic and mechanical properties of three thermoplastic polyimides BPDA-P3, ODPA-P3 and aBPDA-P3 are simulated using the atomistic molecular dynamics technique. The correlation between the dynamic fragility and the polyimides strain-hardening moduli are observed.